13th International Conference on
Structural Health Monitoring of Intelligent Infrastructure
DOI: 10.3217/978-3-99161-057-1-031

Monitoring Timber Structures with Fiber Optics Sensors: State of the Art and Application to a Timber Beam

R. Mansilla-Ruiz[1, 0009-0004-2617-7303], I. Paya-Zaforteza[1, 0000-0002-3995-8772], E. García-Castillo[1,0000-0003-4665-730X], P.A. Calderón-García[1, 0000-0002-9783-9333]
[1]Instituto Universitario de Investigación de Ciencia y Tecnología del Hormigón (ICITECH), Universitat Politècnica de València, Camino de Vera S/N, 46022 Valencia, Spain
email: romanrui@upv.edu.es, igpaza@cst.upv.es, esgarcas@upv.es, pcaldero@cst.upv.es

ABSTRACT: Fiber optic sensors (FOS) offer compelling advantages for Structural Health Monitoring (SHM). However, their application in timber structures remains underexplored. This article reviews the state-of-the-art use of FOS in timber structures and presents an experimental study conducted at the Universitat Politècnica de València. A 3-meter-span timber beam was subjected to a four-point bending test and instrumented with long-gauge strain FOS. The measured strains were used to derive stresses, which were then compared to theoretical values. The results highlight the potential of FOS for accurate stress monitoring in timber elements and contribute valuable insights to the advancement of SHM in sustainable construction.

KEYWORDS: Timber structures; Historic structures; Fiber optic sensors; Strain monitoring; Stress.

1 INTRODUCTION

The built environment is responsible for approximately 39% of global energy-related CO_2 emissions, of which about 11% arises from embodied emissions—those generated during the production, transportation, and installation of building materials [1]. Shifting towards a Circular Economy model is increasingly recognized as essential to mitigate this impact. Among the strategies, the rehabilitation and reuse of existing structures plays a critical role. Among the different potential construction materials, timber stands out as a sustainable material due to its low carbon footprint, high recyclability, and significant cultural value, especially in heritage buildings (see e.g. Figure 1).

Figure 1. Timber beams at “Estació del Nord”, a train station in Valencia, Spain.

Structural Health Monitoring (SHM) is a key enabler of sustainable rehabilitation strategies. SHM techniques provide continuous insights into the condition of built structures, which helps to optimize maintenance, supports resource-efficient interventions, and extends service life. Within this context, fiber optic sensors (FOS) present compelling advantages over traditional electrical sensors, offering immunity to electromagnetic interference, high sensitivity, and multiplexing capabilities [2]. Despite growing interest in sustainable rehabilitation methods, the application of FOS in timber structures remains limited and underexplored. Most existing SHM studies have focused on concrete and steel, with relatively few addressing timber. This research seeks to fill that gap by experimentally evaluating the performance of long-gauge FOS in monitoring strain and stress distributions in a timber beam subjected to bending. The main objective is to assess the feasibility and accuracy of using FOS for SHM in timber structures, particularly in heritage or rehabilitated buildings.

The paper is structured as follows: Section 2 briefly reviews the state of the art in fiber optic monitoring of timber structures. Section 3 describes the experimental setup and testing procedure. Section 4 presents the experiment results and Section 5 discusses the performance of FOS in timber. Finally, Section 6 summarizes the main findings and outlines directions for future research.

2 REVIEW OF THE CURRENT STATE OF THE ART

Early explorations of fiber optic sensing in timber structures began with Sargent (2009) [3], who used Fabry–Perot interferometric FOS to monitor temperature during the kiln drying of radiata pine boards, confirming the method’s accuracy but also highlighting sensor fragility under extreme conditions. Marsili et al. (2017) [4] applied Fiber Bragg Gratings (FBGs) to both small specimens and historic timber beams (before and after carrying out a strengthening operation), successfully measuring strain and damping, and demonstrating the potential of FBGs for both laboratory and field applications. Expanding on structural monitoring and reinforcement assessment, Li et al. (2018) [5] instrumented Chinese traditional timber structures, including mortise-tenon joints, using FBGs to effectively track beam deflections and column inclinations under load. Further advancing this line of research, Helmer-Smith et al. (2021) [6] tested a scaled timber Warren truss monitored with distributed fiber sensors (DFOS),

DOI: 10.3217/978-3-99161-057-1-031

successfully capturing strains, and highlighting the capabilities of FOS in truss systems.

More recently, advanced applications have focused on distributed sensing and bond-slip monitoring. Ernewein and Woods (2023) [7] used DFOS to study glued-in steel rods within glulam elements during pull-out tests, capturing detailed strain distributions and bond-slip behavior that surpassed the resolution of traditional strain gauges. Extending DFOS application, Felicita et al. (2024) [8] instrumented timber foundation piles and monitored the stress distribution along their length, validating DFOS accuracy and showcasing its potential for buried timber elements.

3 EXPERIMENT DESIGN

3.1 Loading Set-Up

To evaluate the capability of FOS in monitoring the behavior of timber beams under bending, a four-point bending test was conducted, as shown in Figure 2. A sawn timber beam, graded as C18 according to the Spanish code [9], was placed on two hinged supports to simulate a simply supported condition The dimensions of the steel plates at the supports that were in direct contact with the timber beam were 180x180x40 mm. The load was applied using a hydraulic jack placed at the center of a rectangular steel spreader beam, which transferred the force to two loading points spaced 1 meter apart. Steel plates measuring 85 mm in width and 3 mm in thickness were placed on the top surface of the timber beam at these two points to facilitate uniform load application. The total length of the tested beam was 3400 mm, with a span of 3000 mm. The beam had a depth (*h*) of 202 mm and a width (*b*) of 75 mm.

3.2 Equipment installed

The beam's vertical displacements were recorded using two linear variable differential transducers (LVDTs). Additionally, five long-gauge strain sensors were installed on the beam using brackets screwed into the timber. Table 1 provides the detailed positions of these sensors. The gauge length of the FOS was 500 mm. Figure 3 shows the position of the sensors installed for the test, both LVDTs and FOS. Figure 4 shows a detail of the elements used to distribute the load to the beam, while Figure 5 and Figure 6 provide a detailed view of the long-gauge sensors installed at sections S1 and S2.

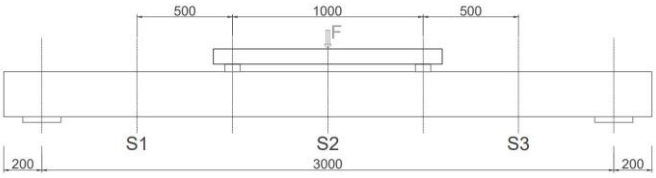

Figure 2. Loading set-up. Position of the monitored cross sections.

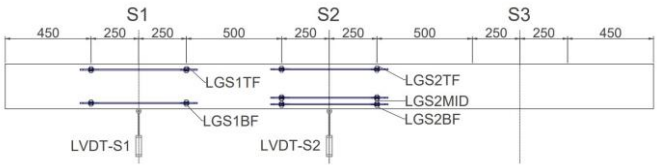

Figure 3. Sensors installed in the tested beam.

Table 1. Specifications for the sensors installed.

Sensor ID	Measuring units	Related section	Position
LVDTS2	mm	S2	Mid-span
LVDTS1	mm	S1	1 m from mid-span
LGS2TF	microstrains	S2	27.88 mm from the beam's top face
LGS2BF	microstrains	S2	26.58 mm from the beam's bottom face
LGS2MID	microstrains	S2	57.54 mm from the beam's bottom face
LGS1TF	microstrains	S1	30.48 mm from the beam's top face
LGS1BF	microstrains	S1	30.05 mm from the beam's bottom face

Figure 4. Central segment of the tested beam showing the loading elements.

DOI: 10.3217/978-3-99161-057-1-031

Figure 5. FOS installed in Section S2.

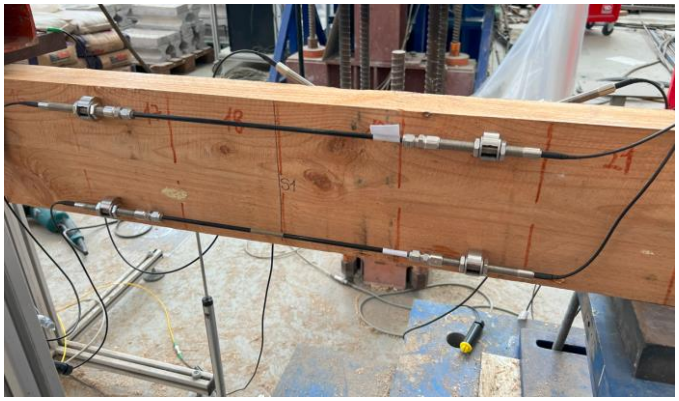

Figure 6. FOS installed in Section S1.

4 RESULTS

This section presents the results obtained from monitoring the timber beam during the bending test. A step-loading protocol was employed, in which the load was incrementally increased to predefined thresholds and then held constant to allow for stabilization. Displacement control was displacement-driven, with a constant loading rate of 0.05 mm/s.

Figure 7 displays the force applied by the hydraulic jack over time, along with the displacements recorded by the LVDTs, plotted on a secondary vertical axis. The curves follow the same trend, showing that the displacements increase proportionally with the applied force. The number of steps in the displacement curves corresponds exactly to the loading steps of the applied force. The maximum recorded force was 11.19 kN, which resulted in LVDT displacements of 7.18 mm at Section S2 (LVDTS2) and 4.99 mm at Section S1 (LVDTS1).

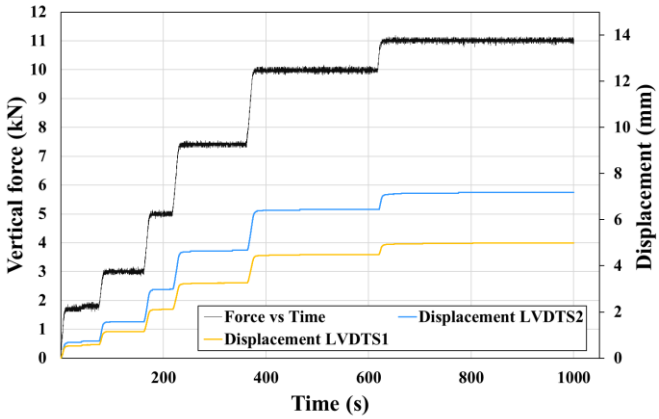

Figure 7. Force and LVDT displacements over time during the bending test.

Figure 8 and Figure 9 display the strain curves recorded by each long-gauge sensor throughout the test. Sensors installed below the geometric centroid of the beam cross section are expected to record tensile strains (negative values), while those positioned above the geometric centroid should register compressive strains (positive values). As expected, sensors LGS1TF and LGS2TF, both located above the geometric centroid, measured compressive strains and sensors LGS1BF, LGS2BF and LGS2MID measured tensile strains.

A comparison of the curves also shows that, as expected, the further a sensor is from the geometric centroid of the cross section, the greater the strain it experiences. Additionally, sensors positioned at the mid-span of the beam experienced higher strain levels than those located at Section S1, which is nearer to the support.

More specifically, the maximum recorded compressive strain at Section S2 was 590 με, while the maximum tensile strain reached 502 με. Sensor LGS2MID, located closer to the geometric centroid recorded a maximum strain of 277 με. LGS2BF recorded a strain 1.81 times greater than that of LGS2MID.

In contrast, the FOS located at Section S1 recorded significantly lower strain values, with a maximum compressive strain of 269 με and a maximum tensile strain of 155 με. This notable difference highlights the effect of the bending moment distribution along the beam. Since Section S2 is in the segment of the beam where the bending moment is at its maximum, higher strain values are expected and observed. Conversely, Section S1, being nearer to the supports where the bending moment is lower, experiences lower strain levels.

DOI: 10.3217/978-3-99161-057-1-031

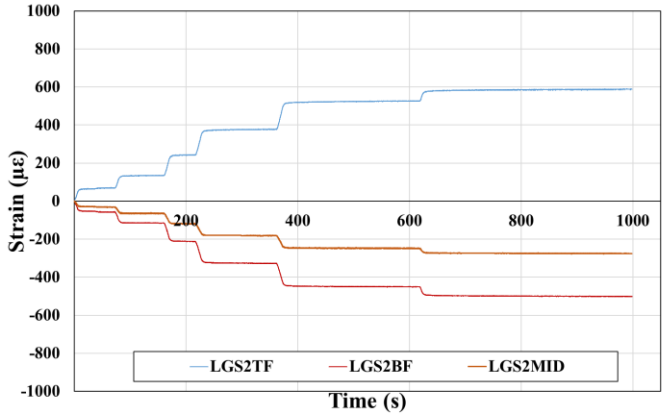

Figure 8. Strain curves for the long-gauge fiber optic sensors installed at S2.

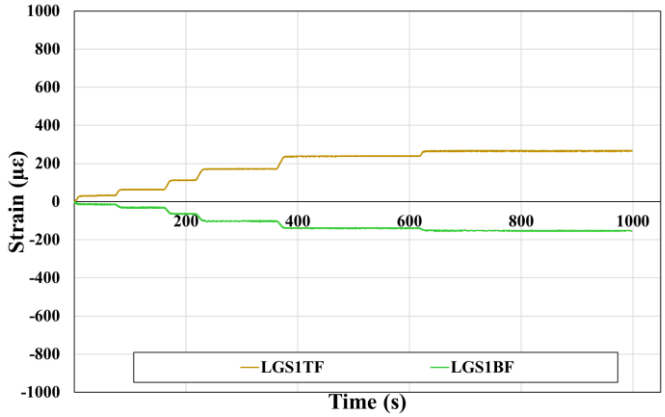

Figure 9. Strain curves for the long-gauge fiber optic sensors installed at S1.

5 DISCUSSION

5.1 Determination of the modulus of elasticity

To validate the use of fiber optic sensors (FOS) in this test, experimental stress values are compared to their theoretical counterparts.

Theoretical stresses are calculated using Equation 1, while experimental stresses are derived from Equation 2. In both equations, σ represents the tensile or compressive stress (in N/mm²). In Equation 1, M is the bending moment at the cross-section (N·mm), I is the moment of inertia of the cross-section (mm⁴), and y is the vertical distance (mm) from the location of the strain measurement to the geometric centroid of the cross-section. In Equation 2, ε is the strain measured by the FOS, and $E_{m,g}$ is the timber modulus of elasticity (in N/mm²).

$$\sigma = \frac{M}{I} y \tag{1}$$

$$\sigma = \varepsilon E_{m,g} \tag{2}$$

The modulus of elasticity $E_{m,g}$ can be obtained either from the Spanish code CTE-DB-SE-M, based on the timber strength class, or measured experimentally according to UNE-EN 408:2011+A1 [10], using the expression shown in Equation 3:

$$E_{m,g} = \frac{3al^2 - 4a^3}{2bh^3\left(2\frac{w2-w1}{F2-F1} - \frac{6a}{5Gbh}\right)} \tag{3}$$

The parameters in this equation are defined as follows:

- a: the distance from a loading point to the nearest support (1 m in this test),
- l: the span between supports (3 m),
- b and h: the width and height of the timber beam, respectively (provided in Section 3),
- F_2 and F_1: two load values within a linear portion of the force–displacement curve (with a correlation coefficient ≥ 0.99),
- w_2 and w_1: the corresponding displacements for forces F_2 and F_1,
- G: the transverse modulus of elasticity, taken from the code for class C18, with a value of 560 MPa.

Using the following values:

- F_2 = 10990 N,
- F_1 = 3200 N,
- w_2 = 7.14 mm,
- w_1 = 1.66 mm,

the calculated value of $E_{m,g}$ is 14577 MPa.

5.2 Stresses at section S1

Experimental stresses calculated for section S1 were compared to their theoretical values, as shown in Figure 10 . The difference between the experimental and theoretical value for LGS1TF accounts for 0.10 MPa, which is negligeable. However, the difference for LGS1BF is 1.59 MPa. More specifically, theoretical calculations provided greater values of tension, but lower compression stress than those obtained from the monitored strains. The maximum theoretical stress values are 3.83 MPa (at the location of the top sensor) and 3.85 MPa (at the location of the bottom sensor), which suggest the exact same stress at the tensioned fibers and at the compressed fibers, and it is justified by the 0.31 mm difference at the installation position in relation to their respective extreme face (top face or bottom face of the beam). However, experimental results of maximum stresses for LGS1TF and LGS1BF locations are 3.93 MPa and 2.26 MPa respectively. These values denote a clear dominance of compression over tension along the length where the sensors are installed for section S1.

At this point it is worth noting that the calculations assumed several hypothesis. Stress calculated with Equation 1 assumes that the material is homogeneous and linear elastic. As it is known for timber, this constitutes a simplification, since it is a heterogeneous material, with varying properties in each direction. Local defects, such as the presence of knots, where the density of the timber grain is higher, and some variability in the direction of the timber fibers can also influence the behavior of the beam under loading, leading to differences between the compression and the tension stresses. Minor differences in the installation of the sensors to the beam can also lead to differences in the results, such as the distance from sensor LGS2TF's axis to the top face of the beam, which is 27.88 mm, while for LGS2BF is 23.54 mm. Accuracy during

DOI: 10.3217/978-3-99161-057-1-031

the installation should be as precise as possible to reduce variability.

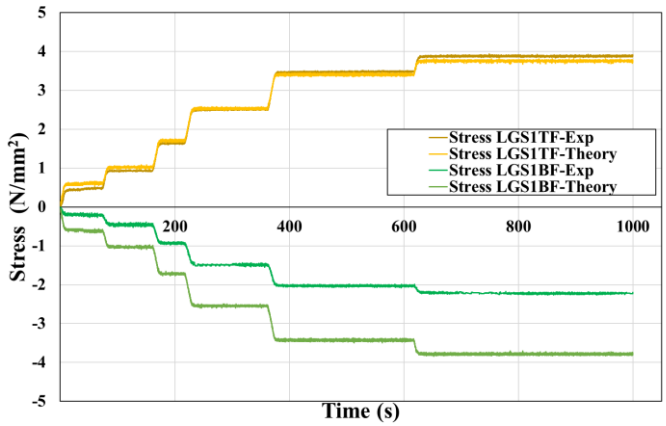

Figure 10. Theoretical stress versus experimental stresses at section S1.

5.3 Stresses at section S2

As shown in Figure 11, differences can be observed between the experimental and theoretical stress values for each long-gauge sensor installed at section S2. These differences are more evident when comparing the stress values at the final loading step (Step 6) of the test.

For sensor LGS2TF, located in the compression zone of the beam, the experimental stress at Step 6 is 0.68 MPa higher than the theoretical value, representing an 8% difference. In the tension zone, for sensor LGS2BF, the theoretical stress exceeds the experimental value by 1.07 MPa, resulting in a 12.75% difference. Similarly, for sensor LGS2MID (also in tension), the theoretical stress is 0.66 MPa greater than the experimental, corresponding to a 14.12% difference. These discrepancies highlight the complexity of comparing real-world measurements with simplified analytical predictions, particularly in anisotropic materials such as timber. In addition, comparing sensors LGS2MID and LGS2BF — both located in the tension zone but at different distances from the centroid — further illustrates the consistency of the results. The maximum recorded strain at LGS2MID was 277 με, while LGS2BF registered 502 με**,** yielding an experimental strain ratio of 1.81 as detailed in Section 4. Using Equation 1 and considering the sensors' relative positions and the maximum applied force of 11.19 kN, the corresponding theoretical stresses are 4.61 MPa for LGS2MID and 8.24 MPa for LGS2BF — a ratio of 1.79. This close agreement between theoretical and experimental ratios supports the validity of the strain measurements and suggests a good correlation between sensor position and measured mechanical response.

To provide a more comprehensive comparison, Table 2 presents the absolute values of experimental and theoretical stresses for loading steps 3 and 6, along with the corresponding percentage differences. All long-gauge sensors were installed within the region of constant bending moment, as defined by the four-point bending configuration, ensuring that there is no uncertainty regarding the bending moment acting on the segment of the beam being analyzed

To ensure the accuracy of theoretical stress calculations, key geometric parameters were precisely measured. The vertical distances (y) from each sensor to the beam's geometric centroid were verified using a digital caliper, and the cross-sectional dimensions of the timber beam were also recorded with high precision. The modulus of elasticity, used to derive experimental stress values from strain measurements, was obtained through an independent experimental procedure following standard guidelines [10]. Therefore, it is not considered a source of significant error in the comparison.

The observed differences are more likely attributed to the natural anisotropy and heterogeneity of timber, including the presence of knots, cracks, grain deviations, or localized density variations. These factors can influence the mechanical response at specific cross-sectional locations and lead to deviations from the idealized behavior predicted by classical bending theory.

Table 2. Comparison of stresses at section S2 for loading steps 3 and 6.

	LGS2TF	LGS2BF	LGS2MID
Experimental stress at step 3 (MPa)	3.52	3.08	1.73
Theoretical stress at step 3 (MPa)	3.61	3.82	2.14
Difference (%)	2.49	19.37	19.15
Experimental stress at step 6 (MPa)	8.54	7.26	4.01
Theoretical stress at step 6 (MPa)	7.78	8.24	4.61
Difference (%)	8.90	11.92	13.99

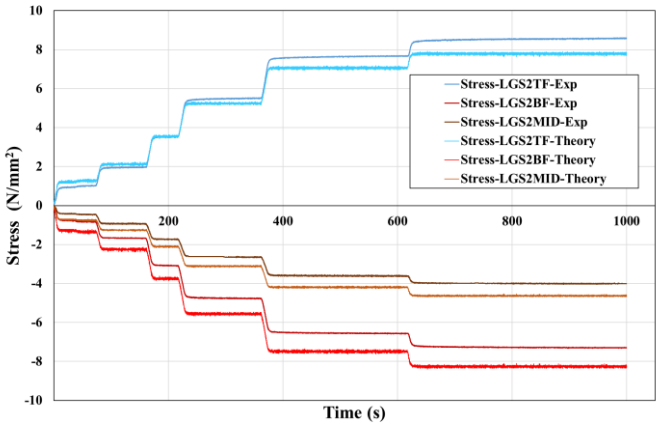

Figure 11. Theoretical stress versus experimental stress at section S2.

6 CONCLUSIONS AND FUTURE RESEARCH

This study focused on monitoring key parameters of a classified timber beam subjected to a four-point bending test, enabling a comparison between stresses derived from strain measurements and theoretical values based on classical strength of materials principles. The following conclusions can be drawn:

- Fiber optic sensors (FOS) are effective tools for monitoring the strain behavior of timber structural elements. The results obtained during testing showed strong agreement with the expected behavior under a step-loading protocol. FOS provided high-resolution strain data, from which stress was reliably derived

DOI: 10.3217/978-3-99161-057-1-031

using appropriate mechanical models and material properties. This capability highlights their value in structural health monitoring (SHM) applications.

- FOS have the potential to detect localized anomalies in material behavior. For example, sensor LGS1TF-Exp exhibited a 58.7% deviation from its theoretically derived stress value, a difference which cannot be overlooked. Possible explanations include the presence of defects—such as knots or abrupt grain deviations—that alter local strain behavior. Installation-related issues may also have contributed to the anomaly.
- Precision in FOS installation is critical. The accuracy of strain measurements is highly dependent on proper sensor alignment, bonding quality, and the technician's skill. Even with optimal procedures, a certain level of uncertainty is inevitable due to the high sensitivity of these sensors (on the order of 2 με), underscoring the importance of meticulous installation and calibration.
- Further research is needed to systematically explore the causes of large deviations between measured and theoretical stress values. The nearly 59% error observed at the location of sensor LG-S1-BF is too large to be attributed solely to timber's natural variability—such as knots, fiber misalignment, or moisture content—though these factors do influence strain-stress correlation. It is therefore likely that some form of installation or operational error occurred. Future work should include defect mapping, and improved sensor validation protocols to try to isolate and quantify these effects.

ACKNOWLEDGEMENTS

This article is part of the grant PID2021-128152NB-I00 funded by MICIU/AEI/10.13039/501100011033 and by ERDF/EU. The authors also wish to acknowledge the support received through the predoctoral grant PRE2022-103404**,** funded by MICIU/AEI/10.13039/501100011033 and by FSE+ (European Social Fund Plus). This grant was awarded to the first author to support his doctoral research.

REFERENCES

[1] World Green Building Council. Bringing Embodied Carbon Upfront: Coordinated Action for the Building and Construction Sector to Tackle Embodied Carbon. 2019.
[2] Torres B, Payá-Zaforteza I, Calderón PA, Adam JM. Analysis of the strain transfer in a new FBG sensor for Structural Health Monitoring [Internet]. Vol. 33, Engineering Structures. Elsevier BV; 2011. p. 539–48. Available from: http://dx.doi.org/10.1016/j.engstruct.2010.11.012
[3] Sargent R. Measurement of Board Temperatures during Kiln Drying Using Fiber Optic Sensors [Internet]. Vol. 37, Journal of Testing and Evaluation. ASTM International; 2009. p. 306–9. Available from: http://dx.doi.org/10.1520/jte101914
[4] Marsili R, Rossi G, Speranzini E. Fibre Bragg Gratings for the Monitoring of Wooden Structures [Internet]. Vol. 11, Materials. MDPI AG; 2017. p. 7. Available from: http://dx.doi.org/10.3390/ma11010007
[5] Li NL, Jiang SF, Wu MH, Shen S, Zhang Y. Deformation Monitoring for Chinese Traditional Timber Buildings Using Fiber Bragg Grating Sensors [Internet]. Vol. 18, Sensors. MDPI AG; 2018. p. 1968. Available from: http://dx.doi.org/10.3390/s18061968
[6] Helmer-Smith H, Vlachopoulos N, Dagenais MA, Forbes B. Comparison of multiple monitoring techniques for the testing of a scale model timber Warren truss [Internet]. Valsangkar A, editor. Vol. 6, FACETS. Canadian Science Publishing; 2021. p. 1510–33. Available from: http://dx.doi.org/10.1139/facets-2021-0001
[7] Ernewein B, Woods JE. Distributed fiber optic strain sensing in axially loaded glued-in steel rods in glued-laminated timber [Internet]. Vol. 392, Construction and Building Materials. Elsevier BV; 2023. p. 132020. Available from: http://dx.doi.org/10.1016/j.conbuildmat.2023.132020
[8] Felicita M, Pagella G, Ravenshorst G, Mirra M, van de Kuilen JW. Assessment of in-situ stress distribution and mechanical properties of wooden foundation piles instrumented with distributed fiber optic sensors (DFOS) [Internet]. Vol. 20, Case Studies in Construction Materials. Elsevier BV; 2024. p. e03139. Available from: http://dx.doi.org/10.1016/j.cscm.2024.e03139
[9] Código Técnico de la Edificación. Documento Básico SE-M Seguridad Estructural - Madera. Ministerio de Fomento, España, 2019.
[10] UNE-EN 408:2011+A1. Timber structures - Structural timber and glued laminated timber - Determination of some physical and mechanical properties. AENOR, 2011+A1